Thermomechanical Properties and Oxidation Resistance of Zirconia CVI-Matrix Composites: 1—Mechanical Behavior

J. Minet,* F. Langlais,‡ J. M. Quenisset & R. Naslain†

Laboratoire de Chimie du Solide du CNRS, Université de Bordeaux
351, Cours de la Libération, 33405-Talence, France

Abstract

The mechanical behavior of various zirconia-based fibrous composites has been studied at ambient and high temperatures. The composites were prepared by ZrO_2-CVI densification, from preforms made of alumina or carbon fibers consolidated with a small amount of alumina, pyrocarbon or hex-BN. When loaded under compression at room temperature, 2D-C-C/ZrO_2 composites exhibit mechanical behavior similar to that already reported for the related 2D-C-C/SiC, 2D-C-C/B_4C, 2D-C-C/TiC or 2D-C-C/BN materials with: (i) a linear elastic domain, (ii) a damaging domain prior to failure and (iii) an anisotropy which decreases as $V(ZrO_2)$ is raised. Under three-point bending, the alumina–zirconia composites behave, at room temperature, in a non-brittle manner when the preform has been consolidated by BN, with crack deviation and pull-out phenomena. The variations of the stiffness and strength versus $V(ZrO_2)$ obey exponential laws at room temperature. Finally, the alumina–zirconia composites keep their strength and rigidity up to about $1000°C$ under an atmosphere of argon/hydrogen.

Die mechanischen Eigenschaften von verschiedenen faserverstärkten Zirkonoxidverbundwerkstoffen wurden bei Raum- und Hochtemperaturbedingungen untersucht. Die Komposite wurden durch ZrO_2-CVI (Chemical-vapor-infiltration) verdichtet, wobei von vorgeformten Aluminiumoxid- oder Kohlenstoffasern ausgegangen wurde, die mit kleinen Gehalten von Al_2O_3, *Pyrokohlenstoff oder hexagonalem BN vorverfestigt waren. Bei einer Druckbelastung bie Raumtemperatur zeigten die 2D-C-C/ZrO_2-Verbundwerkstoffe ein ähnliches mechanisches Verhalten wie 2D-C-C/SiC-, 2D-C-C/B_4C-, 2D-C-C/TiC- oder 2D-C-C/BN-Werkstoffe mit: (i) einem linear elastischen Bereich, (ii) einem Bereich der Schädigung vor dem Versagen und (iii) einer Anisotropie, die in dem Maß abnimmt, wie das ZrO_2-Volumen ansteigt. Beim Raumtemperatur-3-Punktbiegeversuch verhalten sich die* Al_2O_3–ZrO_2-*Vergundwerkstoffe nicht spröde mit Rißablenkung und 'pull-out'-Verhalten, wenn das Fasergelege mit BN vorverfestigt war. Die Änderung der Steifigkeit und der Festigkeit in Abhängigkeit vom ZrO_2-Gehalt gehorcht bei Raumtemperatur exponentiellen Gesetzen. Die Aluminium–Zirkonoxid-Verbundwerkstoffe behalten bis ca. $1000°C$ ihre Festigkeit und Steifigkeit in einer Argon/Wasserstoff-atmosphäre bei.*

Le comportement mécanique de divers composites fibreux à base de zircone, a été étudié à l'ambiante et à haute température. Les composites étaient préparés par densification CVI à l'aide de zircone, à partir de préformes constituées de fibres d'alumine ou de carbone et consolidées à l'aide d'une petite quantité d'alumine, de pyrocarbone ou de BN-hexagonal. Les composites 2D-C-C/ZrO_2, sollicités en compression à température ambiante, ont un comportement mécanique similaire à celui déjà observé pour les matériaux voisins 2D-C-C/SiC, 2D-C-C/B_4C, 2D-C-C/TiC ou 2D-C-C/BN avec: (i) un domaine de déformation élastique, (ii) un domaine d'endommagement avant la rupture et (iii) une anisotropie qui décroît quand $V(ZrO_2)$ augmente. En flexion 3 points, les composites alumine–zircone se comportent, à température

* Present address: Société Européenne de Propulsion, BP 37, F 33165 Saint Médard-en-Jalles.
‡ Present address: Laboratoire des Composites Thermo-structuraux (UMR 47 CNRS-SEP-UB1), 1–3, Avenue Léonard de Vinci, Europarc, F 33600 Pessac.

ambiante, de manière non-fragile quand la préforme a été consolidée par BN, avec phénomènes de déviation de fissures et de déchaussement de fibres. Les variations de la rigidité et de la résistance en fonction de $V(ZrO_2)$ suivent des lois exponentielles à température ambiante. Finalement, les composites alumine-zircone conservent leur résistance et leur rigidité jusqu'aux environs de 1000°C sous une atmosphère d'argon/hydrogène.

1 Introduction

It is now well established that the fiber composite concept provides an efficient way to improve the toughness and reliability of engineering ceramics. Very recently, the key role played by the fiber–matrix interfaces (or interphases) in the mechanisms which control the crack propagation (and thus, the failure and fracture work) of the ceramic matrix composites (CMC) has been identified for different fiber–matrix ceramic couples. It appears that tough composites are obtained when the fibers are not too strongly bound to the matrix allowing thus different energy-absorbing phenomena to take place (e.g. compliant load transfer at the fiber–matrix interface, fiber friction against the matrix and, finally, fiber pull-out) under loading. It has been shown that a way to control crack propagation in CMC is to add a thin layer of a compliant material (e.g. pyrocarbon or hex-BN), at the fiber–matrix interfaces, either through an in-situ reaction occurring at high temperatures during the elaboration of the composites or as a coating applied to the fibers prior to their insertion in the matrix.[1-4] However, these interphases are sensitive to oxidation, and experimental data showing the dependence of the strength of such composites on test atmospheres have been already given.[5] Therefore, the behavior of CMC with respect to long exposures at high temperatures in oxygen-containing atmospheres is an important subject for the future of CMC.

The aim of the present work was to explore the potential of zirconia as a ceramic matrix in CMC for aerospace applications at high temperatures. On the basis of the above general considerations, zirconia has several advantages with respect to carbon and SiC: (i) it is a very refractory compound ($T_m \approx$ 2700°C) and stable oxide, (ii) it is a good insulating material whereas both graphite and SiC exhibit a high thermal conductivity and (iii) it undergoes a polymorphic transition, $ZrO_{2(m)} \rightleftharpoons ZrO_{2(t)}$, with a martensitic character which has been used to increase the toughness of many ceramics. Further-

more, it has been established recently that ZrO_2-based composites can be prepared, at moderate temperatures (i.e. about 900°C), according to the so-called chemical vapor infiltration (CVI) process already used by Colmet *et al.* to prepare Al_2O_3-based composites.[6-9]

Surprisingly, ZrO_2-matrix composites reinforced with continuous fibers have not yet been the subject of much research whereas many articles have been published on the fiber reinforcement of SiO_2-based glass-ceramics, mullite and alumina.[5,9,10] As a matter of fact, when the present study was started, no paper had been devoted to the subject, at least to our knowledge. In the meantime, Pujari and Jawed[11] reported the results of their study on chopped alumina fiber–TZP matrix composites prepared according to a conventional powder metallurgy route. They found that the alumina fibers did result in a twofold increase in toughness with respect to the monolithic TZP but mentioned that the failure mode remained brittle. Almost simultaneously, Bender *et al.*[2] succeeded in preparing ZrO_2–SiO_2 and ZrO_2–TiO_2 matrix composites reinforced with uncoated or BN coated SiC fibers, according to a liquid route (organometallic precursors). They showed that the composites exhibited brittle failure when reinforced with uncoated SiC fibers due to a strong fiber–matrix bonding whereas they did behave in a non-brittle manner with BN-coated SiC fibers, the BN layer allowing the fiber pull-out to occur and preventing the fibers reacting with the matrix. Finally, a few articles were also published on the related whisker reinforced ZrO_2 composites.[12-14]

Our contribution, presented as two companion papers, is a continuation of three articles which have been already published on the synthesis of ZrO_2-matrix composites by CVI.[7-9] The first part of our present contribution gives the results of our work on the mechanical behavior, at ambient and high temperatures, of some ZrO_2-matrix composites reinforced with either alumina or carbon continuous fibers whereas the second part is devoted to their thermal properties and resistance to oxidation.

2 Experimental

The samples used in the present study were prepared, according to a CVI-technique, from five different types of fiber preforms with a marked two-dimensional (or pseudo three-dimensional) character (Tables 1 and 2). Regarding the nature of the potential applications of ZrO_2-matrix composites

Table 1. Mean characteristics of the alumina and carbon fibers used to prepare the preforms

Characteristics	Preforms				
	Saffil alumina fibers (ICI)[16]	Zircar fibers[a]	Sumitomo fibers[17]	Carbon fibers (ex PAN)[b]	Carbon fibers (ex PAN)[b]
Chemical composition	Al_2O_3:96–97 wt% SiO_2:3–4 wt%	Al_2O_3:80 wt% SiO_2:20 wt%	Al_2O_3:85 wt% SiO_2:15 wt%	Treated at 1600°C	Treated at 1600°C
Fiber diam ter (μm)	3	3–5	17	8–10	8·5–9·1
Tensile strength (MPa)	2 000		1 800	2 300	2 300
Tensile failure strain (%)	(0·67)		(0·86)		(0·96)
Young's modulus (GPa)	300		210		240
Fiber length (cm)	1–5	≤5	Continuous	≤15	≤15
Density (g cm^{-3})	3·3	3·1	3·2	1·7–1·8	1·7–1·8

[a] Alumina fibers + silico-aluminous binder for insulating applications (SALI* from Zircar).
[b] Carbon fibers for thermal applications (from Gepem).

and that of the ceramic fibers available when the study was started, two types of reinforcement were selected: (i) alumina based fibers, for their insulating character with a view to applications at medium temperatures in oxygen-rich gas environments and (ii) carbon fibers, for their refractoriness, low coefficient of thermal expansion (CTE) with a view to applications at high temperatures in oxygen-poor gas media. It was understood that this choice might result in fiber–matrix compatibility problems at high temperatures. However, fibers made of pure or stabilized zirconia which would have been more appropriate than alumina fibers were not available at that time nor are they on the market at present.[15]

Different techniques were used to prepare the preforms depending on the nature of the ceramic fibers. Preforms of type 1 were obtained by impregnation of a SAFFIL mat (transition alumina fibers) with an alumina slurry (mean grain size 1 μm), drying and firing at about 1400°C.[16] Preforms of type 2 were supplied by ZIRCAR (made according to a paper industry technique, i.e. from Al_2O_3–SiO_2 fibers in suspension within a liquid medium which was aspirated through a porous substrate, then the fiber cake was dried and fired). Preforms of type 3 were made from a stack of alumina–silica fabrics (from Sumitomo) which were then consolidated with a small amount of hex-BN infiltrated according to a

Table 2. Main characteristics of the preforms and ZrO_2—matrix composites

Characteristics	Composite				
	Type 1 $Al_2O_3(SiO_2)/ZrO_2$	Type 2 $(Al_2O_3$–$SiO_2)/ZrO_2$	Type 3 $2D$-$(Al_2O_3$–$SiO_2)/ZrO_2$	Type 4 $2D$-C-C/ZrO_2	Type 5 p-$3D$-C-C/ZrO_2
Fibers	[a]Al_2O_3:97 wt% SiO_2:3 wt%	[b]Al_2O_3:80 wt% SiO_2:20 wt%	[c]Al_2O_3:85 wt% SiO_2:15 wt%	Carbon ex-PAN	Carbon ex-PAN
Fiber binder	Alumina slurry (1 μm)	Al_2O_3–SiO_2 slurry	Pyro-BN (CVI)	Pyrocarbon (CVI)	Pyrocarbon (CVI)
Texture of the reinforcement	Mat	Short fibers in bulk	2D fabrics stacking	2D fabrics stacking	Pseudo-3D (Novoltex)[d]
Fiber volume fraction (V_f)	0·17	0·10	0·37	0·30	0·20–0·25
Preform porosity (V_{p_0})	0·60	0·85	0·53	0·50	0·70
Preform true density (g cm^{-3})[e]	3·7	3·5	3·25	1·8–1·9	1·8–1·9
Preform apparent density (g cm^{-3})[f]	1·5–1·6	0·5	1·40–1·45	0·90–1·40	0·40
Zirconia volume fraction ($V(ZrO_2)$)	0·44	0·75	0·31	0·38	0·62
Composite apparent density (g cm^{-3})	3·8	4·7	3·2	3·2	4·0

[a] Saffil from ICI.
[b] Alumina fibers + silico-aluminous binder preform from ZIRCAR.
[c] Sumitomo fibers.
[d] Proprietary preform material from SEP.
[e] After grinding.
[f] Mass/apparent volume ratio.

process described in detail elsewhere.[17,18] Preforms of type 4 were a conventional 2D-C-C porous material, i.e. obtained after consolidation of a stack of carbon fabrics (ex-PAN fibers) with a small amount of pyrocarbon deposited by CVI from a natural gas precursor.[19] Finally, preforms of type 5 were of a carbon fiber (ex-PAN) architecture specifically developed by SEP (trade mark Novoltex) and consolidated by pyrocarbon. All the preforms had a marked two-dimensional character (i.e. they were transverse isotropic) except type 5 which were pseudo three-dimensional (i.e. in the Novoltex architecture, some carbon fibers running in a direction perpendicular to the main 2D fiber construction). As shown in Table 2, the open porosity of the preforms after consolidation, V_{po}, range from 50 to 85% and the residual porosity after ZrO_2-CVI densification, V_p, from 8 to 20%.

The densification of the porous preforms with zirconia was performed according to the CVI technique which was first worked out by Christin *et al.* for SiC-based composites and then extended to various CMC (namely B_4C, TiC, BN and, more recently, Al_2O_3 matrices).[20,21] It has been, for the particular case of zirconia, described in detail elsewhere.[6-8] For the purpose of the discussion, it will be sufficient to recall here that the precursor of the matrix is a $ZrCl_4$–H_2–CO_2 mixture, the densification of the preforms being conducted in a CVI laboratory apparatus under the following conditions: $T = 900°C, p = 2\,kPa$ and $D = 100\,cm^3\,min^{-1}$

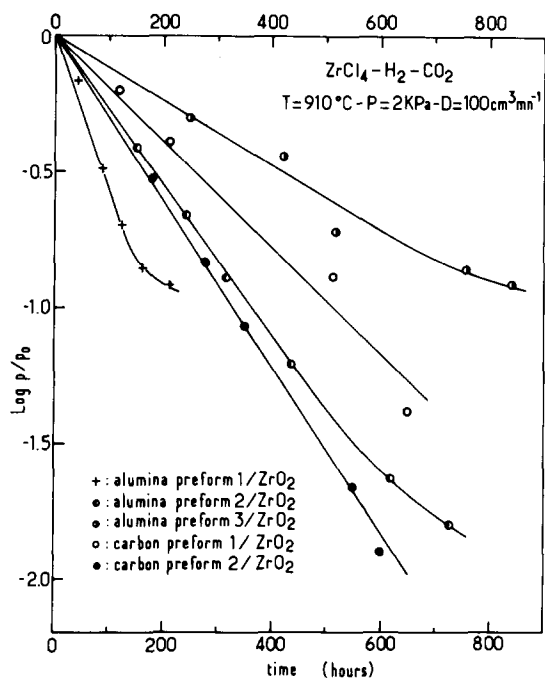(Ref. 8). The kinetics of densification of the preforms are given in Fig. 1 as the variation versus time of $\log p/p_0$, where p_0 and p are respectively the pore volumes at $t = 0$ and at a given infiltration time t. It clearly appears that the infiltration rates remain constant over a large fraction of the overall process duration. However, near the end, i.e. when the residual pore mean diameter becomes too small, a deviation from the linear relationship is usually observed indicating that the pore entrances begin to be obturated, a feature already reported by Rossignol *et al.* for TiC and by Hannache *et al.* for B_4C infiltrations.[22,23] Finally, the infiltration rate depends on the nature of the preform (each preform being characterized by a specific pore spectrum depending on its nature). As shown in Table 2, the residual porosity of the composites after the ZrO_2-CVI step, V_p, ranged from 0·08 to 0·20. No effort was made to attain full densification regarding the time which will have been necessary to reach a residual porosity of less than, say, 0·05. As a result, the volume fraction of zirconia deposited within the pore networks, $V(ZrO_2)$, ranged from 0·30 to 0·75 depending on the nature of the preforms.

The samples used for the mechanical and thermal tests as well as those used to assess the resistance of the composites to oxidation were cut and machined from the consolidated preforms, in different directions with respect to the fiber layers, as shown in Fig. 2, and then densified with zirconia (up to increasing $V(ZrO_2)$ values). No machining or surfacing treatments were performed after the CVI-densification step.

The compression tests were performed on cylindrical specimens ($d = 8\,mm$; $h = 16\,mm$), the load being applied along the directions 1 or 3. The tests were performed with two different displacement speeds, i.e. 0·1 mm min^{-1} for direction 1 and 1 mm min^{-1} for direction 3, since in 2D composites the corresponding rupture strains are not within the same range of values, as discussed below. Due to the small size of the specimens, the approximation of the specimen deformation through the machine

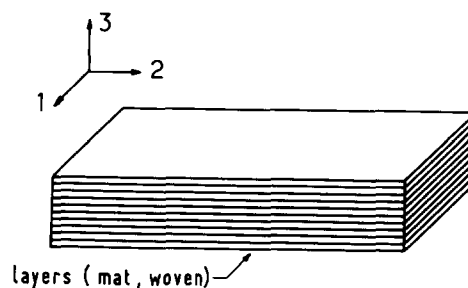Fig. 1. Zirconia infiltration kinetics of the fibrous porous preform.

Fig. 2. Definition of the materials' natural directions.

displacement means considering the Young moduli measured under compression as comparative rather than true values.

The bending tests were performed on specimens with a rectangular cross-section ($12 \times 2\,mm^2$) and a length of 50 mm. The specimen length and width correspond to the composite directions 1 or 2, the load being applied in direction 3 according to a three-point bending test configuration (span: 40 mm). The tests were performed with displacement speeds of $0\cdot1\,mm\,min^{-1}$ at room temperature and $1\,mm\,min^{-1}$ at high temperatures (under a protective gas atmosphere of argon containing 5 vol. % of hydrogen at a total pressure of 400 mbar).

For some of the specimens, the Young's modulus E_1 was measured, between room temperature and 1200°C with a Grindo Sonic Apparatus, by determining the frequency of propagation of acoustic waves along direction 1 of samples 50 mm in length with a square cross-section ($5 \times 5\,mm^2$). The Young's modulus is given by :

$$E_1 = \rho C_1^2 \tag{1}$$

where C_1 is the velocity of the tensile wave applied in the direction 1 of the composite and ρ the density.

3 Results and Discussion

3.1 Comparative behavior under compression loading

The mechanical behavior of the $2D\text{-}C\text{-}C/ZrO_2$ (composites of type 4) were studied under compression loading, in both directions 1 and 3, by testing at room temperature 25 specimens whose zirconia volume fractions ranged from 0 to $0\cdot35$ (the initial porosity of the 2D-C-C preform being of the order of $0\cdot45$). As shown in Figure 3, the stress–strain curves exhibit general features which are typical of 2D ceramic composites.[24,25] Their analysis can be done on the basis of three strain domains:

(i) For $0 < \varepsilon < \varepsilon^A$, a first domain (I), which is particularly limited in direction 3 and for materials with high volume fractions of zirconia, is related partly to the non-linearity of the loading system and, to some extent, to small rearrangements within the fibrous structure. As already discussed elsewhere, the distinction between these two effects is rather complex when the specimens are small and it is not required for a first approach of the mechanical behavior.[26]
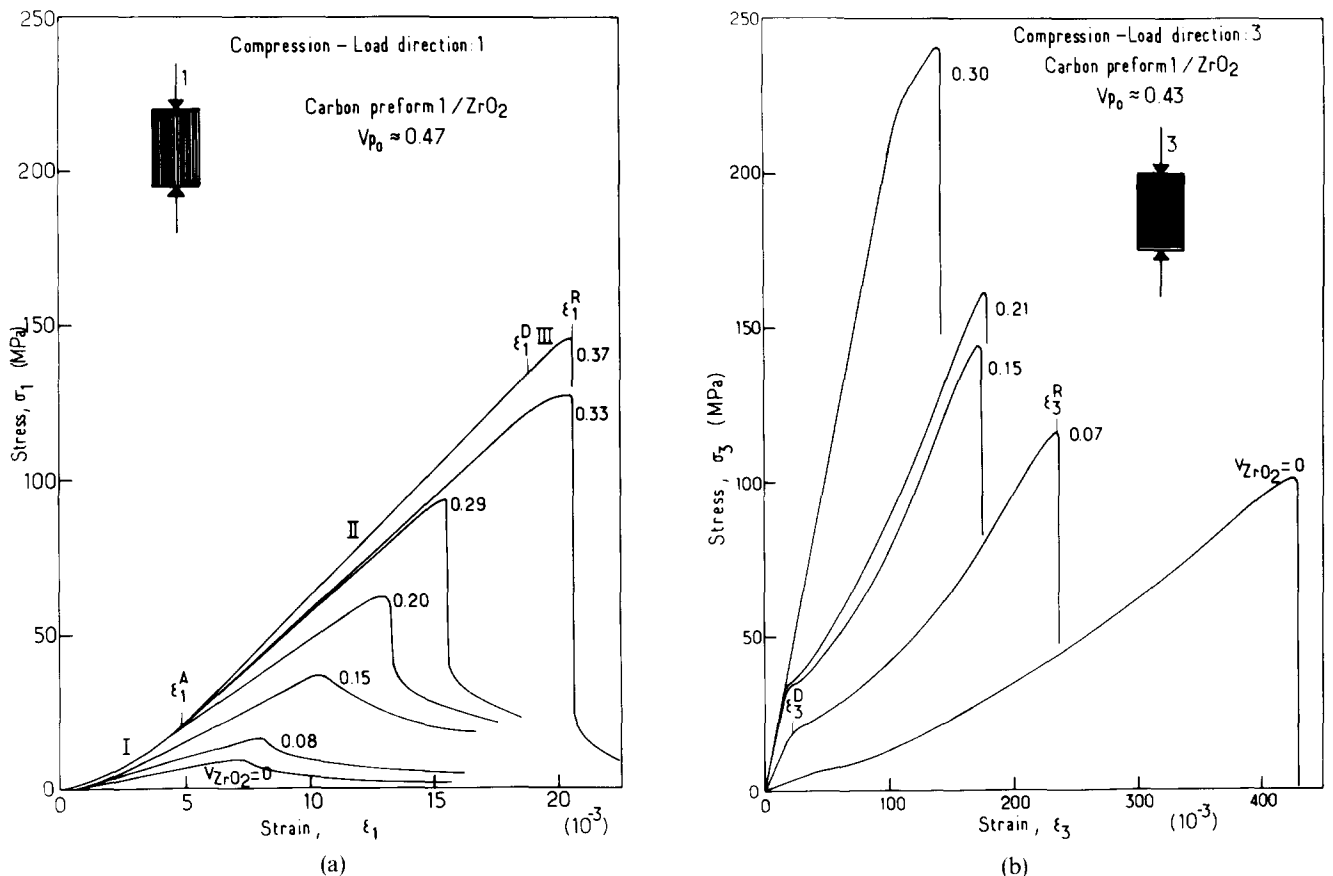

Fig. 3. Compression behavior of $2D\text{-}C\text{-}C/ZrO_2$ (composites type 4). (a) Load applied in direction 1; (b) load applied in direction 3.

(ii) For $\varepsilon^A < \varepsilon < \varepsilon^D$, a second domain (II) corresponds to linear elastic behavior up to a yielding or damaging stress which strongly depends on $V(ZrO_2)$. The elastic characteristics of the materials which are discussed below were derived from this domain.

(iii) For $\varepsilon^D < \varepsilon < \varepsilon^R$, a third domain (III) of non-linear behavior leads to the rupture of the materials and is related to the occurrence of damaging mechanisms within the brittle matrix. The width of this domain is quite different depending on the loading direction. In direction 3 and for incompletely densified materials this domain is so broad that it seems to correspond to a 'strain hardening' effect. In fact, the damaging mechanisms related to the non-linear parts of the stress–strain curves correspond to a decrease in the material rigidity due to matrix micro-cracking. The apparent increase in stiffness, observed in Fig 3(b), as strain increases, is the result of the compaction of the fabric layer stacking after an extensive degradation of the ceramic matrix.

Thus, the general features of the mechanical behavior of 2D-C-C/ZrO_2 composites are very

similar to those already reported for other 2D-C-C/ceramic composites (where the CVI matrix can be: carbon, SiC, SiC + C, TiC, BN or B_4C).[24,25] This result shows how predominant is the contribution of the reinforcement architecture (which is the same for all these materials) in the mechanical behavior of the composites compared to the influence of the nature of the matrix.

The evolution of the Young's moduli E_1 and E_3 over the range of zirconia volume fractions achieved, shows a strong increase in rigidity as $V(ZrO_2)$ is raised (Fig. 4). It can be fitted with an exponential function as proposed by Spriggs[26] as well as by a parabolic law as suggested by Rossignol *et al.*[25] It is noteworthy that the gap between E_1 and E_3 is progressively reduced as the composites become more isotropic with increasing zirconia volume fractions. Although the maximum values which have been reached, for a residual porosity of 10% (i.e. for $V(ZrO_2) = 0.35$), are only of the order of 35 GPa for E_1 and 10 GPa for E_3 (and probably more due to the roughness of the measurements), much higher rigidities could be expected from an improvement in the densification level.

Regarding the yielding and rupture stresses, the two different orthotropic directions should be considered separately since, on one hand, the
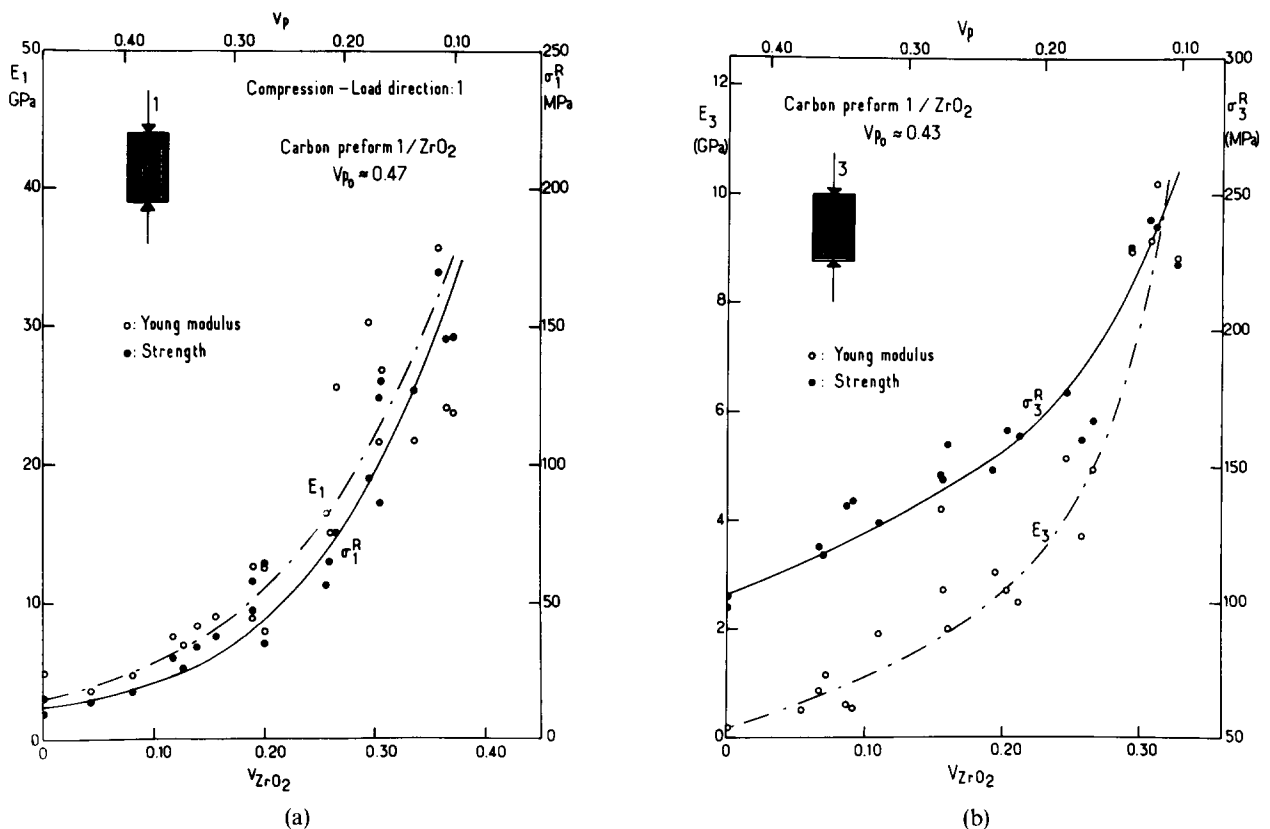

(a)   (b)

Fig. 4. Variations of the Young's modulus (E) and the stress to failure (σ_R) of 2D-C-C/ZrO_2 composites (composites type 4) as a function of zirconia volume fraction $V(ZrO_2)$. (a) Load applied in direction 1; (b) load applied in direction 3.

yielding stresses are very close to the maximum stresses in direction 1, on the other hand, the gap between these two stress levels is quite high in direction 3. However, the evolution of all these parameters versus porosity, which is illustrated in Fig. 4, can be represented by the following general function, as proposed independently by Duckworth and by Rossignol *et al.*[25,27,29]:

$$\sigma = \sigma(o)\exp - K_\sigma V_p \qquad (2)$$

where σ is either the yielding stress σ_3^D or the rupture stress (σ_1^R or σ_3^R), $\sigma(o)$ is the value of the yielding or rupture stress extrapolated to complete densification (i.e. $\sigma_3^D(o) = 330$ MPa; $\sigma_3^R(o) = 280$ MPa; $\sigma_1^R(o) = 367$ MPa) and K_σ is a fitting constant ($K_3^D = 9.70$; $K_3^R = 2.27$; $K_1^R = 7.65$). Otherwise, the maximum compression stresses achieved for $V_p = 0.10$ (i.e. $V(ZrO_2) = 0.35$) are $\sigma_1^R = 160$ MPa in a direction parallel to the fiber layers and $\sigma_3^R = 235$ MPa in a perpendicular direction. In this latter direction, the stress level above which damaging occurs is low except at the highest densifications which give the 2D-C-C/ZrO_2 composites similar behavior in both directions 1 and 3.

The main difference in the material behavior

under compression loading, between its two orthotropic directions, concerns the damaging (or yielding) strains ε_1^D and ε_3^D as well as the rupture strains ε_1^R and ε_3^R. When the compression load is applied in direction 1, the instability of the fibrous layers of the material leads to buckling phenomena, initiates microcracks within the brittle zirconia matrix and finally results in interlayer delamination. Thus, increasing $V(ZrO_2)$ improves the buckling resistance of the fibrous layers so that failure, which occurs only by interlayer delamination, is delayed towards higher rupture strains ε_1^R. As illustrated in Fig. 5(a), this effect also results in an increase in ε_1^D as $V(ZrO_2)$ is raised since each fibrous layer is able to support higher compressive strains before buckling. This effect is still more noticeable as the volume fraction of the pyrocarbon used to consolidate the preform prior to ZrO_2 densification is higher. It has been found to be more pronounced for the 2D-C-C/ZrO_2 composites than for the other 2D-C-C/ceramic composites previously studied (e.g. $\varepsilon_1^R \approx 22 \times 10^{-3}$ for 2D-C-C/ZrO_2 whereas $\varepsilon_1^R \approx 6$–$8 \times 10^{-3}$ for 2D-C-C/ceramic where the ceramic matrix is made of BN, B_4C, SiC or TiC).[25] This feature could also explain the absence of transition in the rupture mode (i.e.
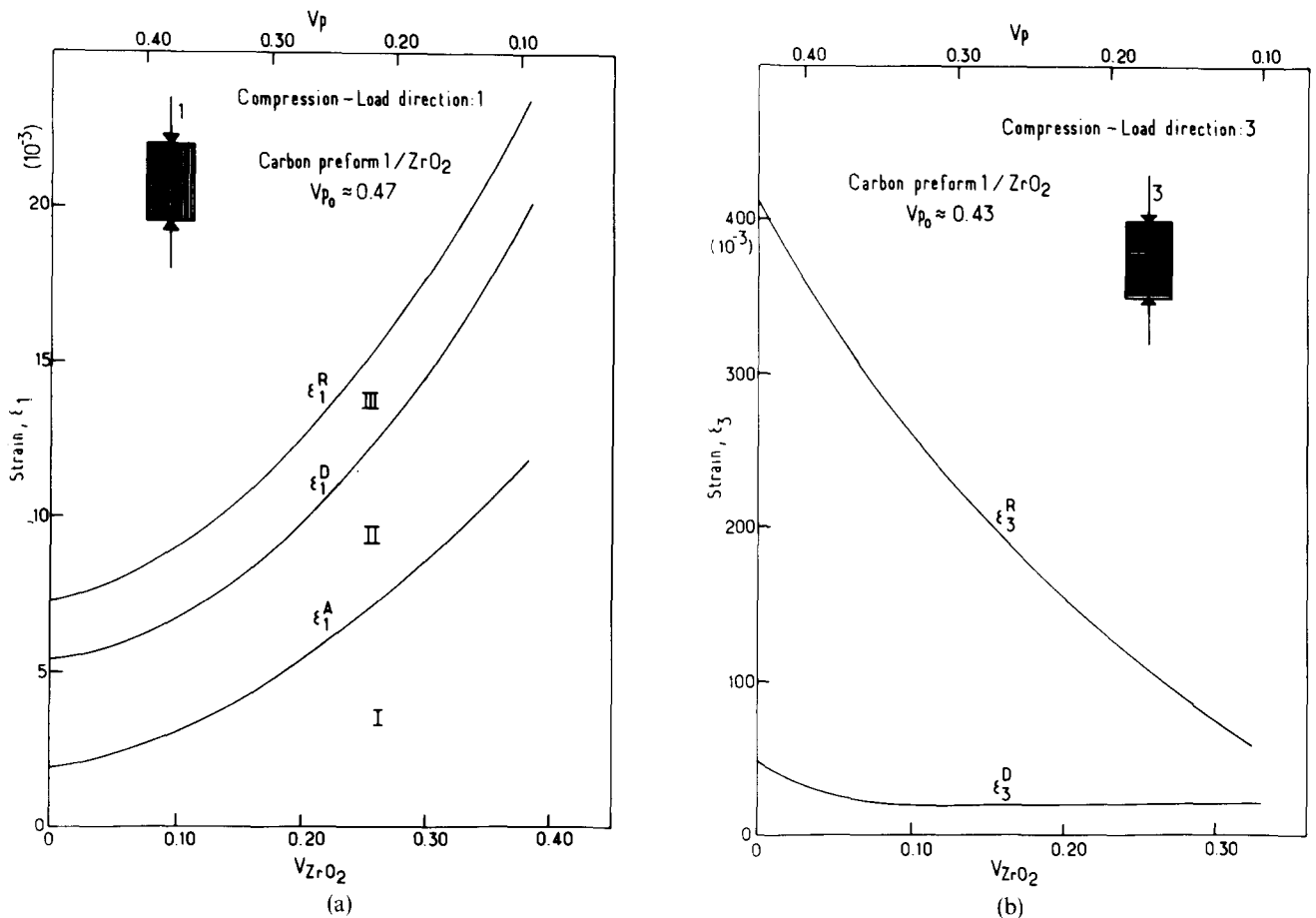

Fig. 5. Variations of the strain ε versus zirconia volume fraction $V(ZrO_2)$ for 2D-C-C/ZrO_2 composites (composites type 4). (a) Load applied in direction 1; (b) load applied in direction 3.

interlayer failure — — → intralayer failure) over the range of zirconia volume fractions which have been achieved: the insufficient zirconia bridging of the fibrous layers prevents any intralayer failure. When the compression load is applied in direction 3, the stability of the structure allows the brittle matrix to be completely crushed into a powder before rupture. The higher the porosity in which the matrix debris can be distributed (i.e. the lower $V(ZrO_2)$), the higher the rupture strain ε_3^R, as illustrated in Fig. 5(b). The damaging initiation corresponds to the fracture strain of the matrix which remains quasi-constant as $V(ZrO_2)$ is raised. On the other hand, it appears that the elastic energy which is required for the matrix microcracking increases as $V(ZrO_2)$ is raised whereas the rupture strain ε_3^R simultaneously decreases. Thus, the compression behavior of $2D\text{-}C\text{-}C/ZrO_2$ composites in direction 3 suggests two contradictory ways for improving the rupture work: (i) an increase in the stress level at failure initiation and (ii) an extension of the failure strain. Finally, it is noteworthy that the compression behaviors of $2D\text{-}C\text{-}C/ZrO_2$ composites in their orthotropic directions (1 and 3) become more and more similar and brittle as $V(ZrO_2)$ increases. On the other hand, the embrittlement seems to be attenuated, at least to some extent, by the presence of the pyrocarbon matrix used to consolidate the carbon fiber preform.
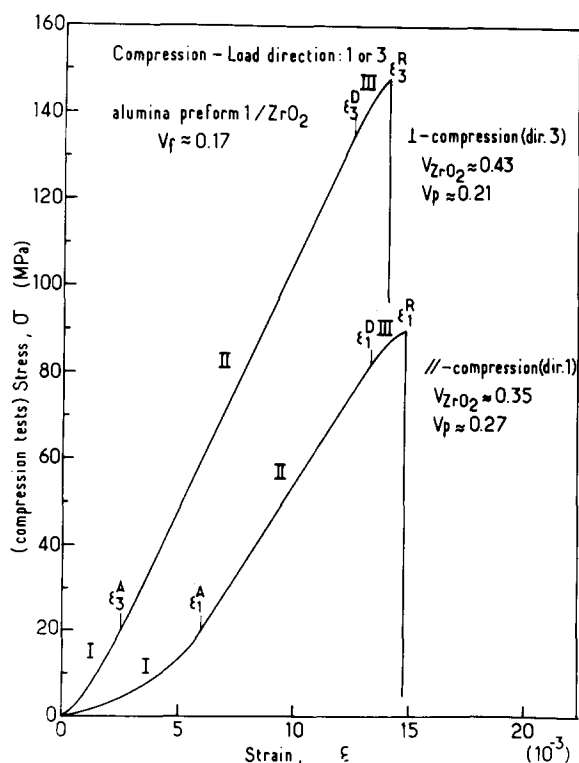
In order to work out, in a similar manner, the role played by the less anisotropic mat preform, the mechanical behavior under compression loading, of the alumina–zirconia composites (type 1) was briefly investigated. The tests were performed on two cylindrical specimens whose axes were respectively orientated along the directions 1 and 3, as shown in Fig. 2. The zirconia volume fractions were 0·35 and 0·43 for the specimens loaded in directions 1 and 3 respectively. As shown in Fig. 6, the stress–strain curves have many common features and their analysis can be done on the basis of three strain domains as already discussed for the $2D\text{-}C\text{-}C/ZrO_2$ composites (Figs 3(a,b)). After a wide stress–strain domain (II) in which the composite is considered to behave as linear elastic, a rather narrow damaging domain (III) is observed prior to failure. This non-linearity indicates the occurrence of microcracking within the brittle matrix which gives rise to a decrease in the rigidity of the material. However, the failure which follows these damaging phenomena remains rather brittle despite the fact that the failure strains are rather high ($\varepsilon_1^R \approx \varepsilon_3^R \approx 15 \times 10^{-3}$). Although the amount of data are still limited, some general aspects of the $Al_2O_3\text{-}ZrO_2$ composites derived from a mat preform can be expected as follows:

(1) The composite rigidity is strongly dependent on the densification level as observed for most ceramic matrix composites obtained by CVI.

(2) The alumina binder and the residual porosity is presumed to impede, at least partly, the notch effects due to the zirconia matrix microcracking, thus slightly delaying the composite fracture. However, the deviations between the yielding and fracture strains recorded for rather low densification levels ($V_p \approx 0·25$) are small enough to think that this type of composite should be quite brittle after complete densification.

(3) The deviation between the failure stress obtained in directions 1 and 3 ($\sigma_1^R \approx 90$ MPa; $\sigma_3^R \approx 150$ MPa) is thought to be more likely related to the difference in densification level rather than the material anisotropy. It is a matter of fact that the predominance of the matrix volume fraction should significantly reduce the contribution of the already moderate anisotropy of the initial preform, giving the composite a quasi-isotropic behavior.

Fig. 6. Compression behavior of composites of type 1 (Saffil fibers + alumina powder (1 μm) preform/ZrO_2 loaded parallely (direction 1) and perpendicularly (direction 3) to fiber layers.

In summary, comparison between $2D\text{-}C\text{-}C/ZrO_2$

composites (type 4) and the alumina–zirconia composites (type 1) leads to the following remarks:

(1) In both cases the performances of these composites are strongly dependent on the densification level.

(2) When on one hand the features of the mechanical behavior related to 2D-C-C/ZrO_2 are quite different depending on the loading directions (1 or 3), the alumina–zirconia composites (type 1) seem to be much less sensitive to the loading direction. Indeed, the toughening effect of the fibrous reinforcement is only effective when the fiber strength and volume fraction are not small compared to those of the matrix.

(3) In direction 3, for a moderate densification level of a 2D-C-C preform, the pores within the carbon network allow an extensive degradation of the zirconia matrix before failure giving rise to significant rupture strain. For high densification level, the carbon network is rigid and resistant enough to delay the matrix microcracking by building up a multiaxial stress field in the matrix. It leads to high yielding and failure strength.

(4) In direction 1, the failure mechanism deals with buckling of carbon fabric layers so that a small content of zirconia or an excessive amount of carbon matrix result in weak interlayer bounding and failure by delamination.

(5) On the other hand, and although the alumina preforms derived from mats are not isotropic, part of the randomly oriented fibers are sufficient to allow macrocracking in any direction. However, the relatively low mechanical performance of the alumina fibers used compared to carbon fibers, the random orientation in mat layers, as well as the presence of alumina powder and porosities at the fiber–matrix interface are thought to facilitate the formation and coalescence of large microcracks occurring in thick zirconia coatings and result in smaller failure strain.

3.2 Effect of the nature of alumina preforms on bending properties

The mechanical behavior, in bending, of the alumina–zirconia composites (types 1, 2 and 3) was studied, at room temperature, as a function of $V(ZrO_2)$. The orientation of the three-point bending specimens with respect to the material directions given in Fig. 2, was the same for all the composites, the load being applied in direction 3. The load–deflection curves are given in Fig. 7(a–c).

It clearly appears from Fig. 7(a,b) that composites of both types 1 and 2 exhibit a brittle character which indicates that the energy dissipation related to damaging mechanisms is not significant enough (as already established under compression loading for composites 1) to prevent the catastrophic propagation of any crack initiated at the specimen surface.
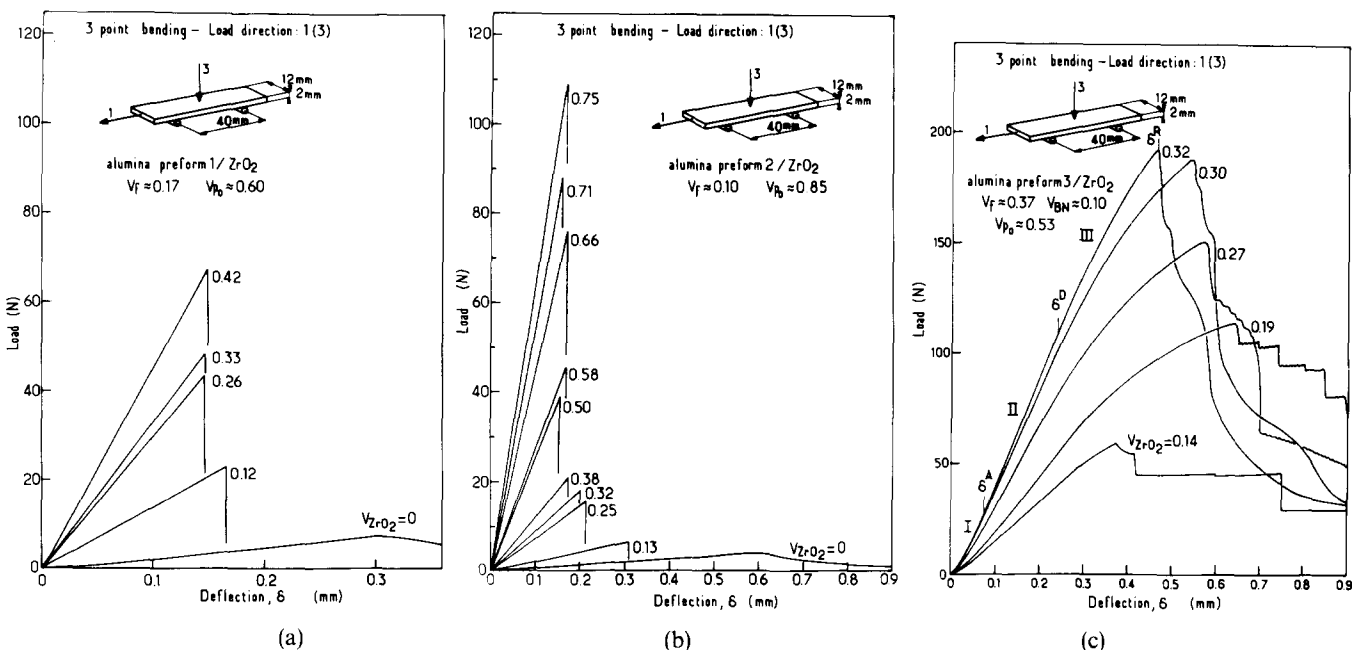

Fig. 7. Three-point bending behavior of (a) composites type 1 (Saffil fibers + alumina powder (1 μm) preform/ZrO_2), (b) composites type 2 (Al_2O_3 fiber + silico-aluminous bonding preform/ZrO_2), (c) composites type 3 (2D-Al_2O_3 (Sumitomo)-BN preform/ZrO_2).

These two types of composites can be regarded as linear elastic. On the other hand, and as shown in Fig. 7(c), composites of type 3 (i.e. a stack of alumina fabrics consolidated with a small amount of hex-BN and more less densified with zirconia) exhibit, after a linear elastic domain II, extensive damaging phenomena within the zirconia matrix which result in a broad non-linear domain III prior to fracture. Thus, the continuous 2D fibrous network can fail progressively, i.e. layer after layer, since the relatively soft BN interphase impedes the microcrack propagation. As a result, the composites of type 3 exhibit an overall non-brittle behavior which contrasts strongly with the brittle behavior of composites types 1 and 2.

As shown in Fig. 8(a,b), the rupture deflections δ^R of the composites of types 1 and 2 decrease with increasing $V(ZrO_2)$ up to a limit of about 0·17 mm (corresponding presumably to the zirconia fracture strain). On the other hand, those observed for composites of type 3 are much higher, as shown in Fig. 8(c). In addition, the load–deflection curves related to composites of type 3 allow a clear distinction between the yielding deflection δ^D which remains almost constant within the $V(ZrO_2)$ range studied and the rupture deflection δ^R whose variation versus $V(ZrO_2)$ is very significant and non-monotonous. This non-monotonous feature could be related to a transition between two rupture mechanisms: (1) up to about $V(ZrO_2) = 0·20$, raising $V(ZrO_2)$ increases the rigidity and strength of the fibrous layers and improves their cohesion so that rupture by delamination is delayed while the

zirconia coating is not yet thick enough to induce notch effects such that matrix microcracks propagate, (2) for $V(ZrO_2) > 0·20$, the notch effects due to matrix microcracking are effective enough to embrittle the whole composite despite the presence of the soft BN interphase. This feature thus results in a decrease in δ^R.

Thus, the major differences in the mechanical behaviors of the three types of alumina fiber–zirconia matrix composites seem to be related, in a first approach, to both the fiber architecture and, as discussed below, the nature of the fiber–matrix bonding.

3.2.1 Variations of the stiffness and rupture strength versus $V(ZrO_2)$

Both the rigidity and rupture strength of composites types 1–3 increase as $V(ZrO_2)$ is raised, as shown in Fig. 9. These evolutions can be depicted on the basis of exponential laws similar to that given above for the compression strength (i.e. eqn (2)) with the values of the constant K and the extrapolated stiffness $E_1(o)$ and strength $\sigma_1(o)$ listed in Table 3. A similar evolution of E_1 versus $V(ZrO_2)$ (with slightly lower E_1 values) has also been observed from the stiffness measurements derived from acoustic wave propagation data (recorded with the Grindo Sonic Apparatus) (Fig. 9(b)). All these results show again the important role played by the related residual porosity-zirconia volume fraction parameters (for composites processed by CVI from a given preform: $V_p + V(ZrO_2) = V_{p_o} = $ constant).
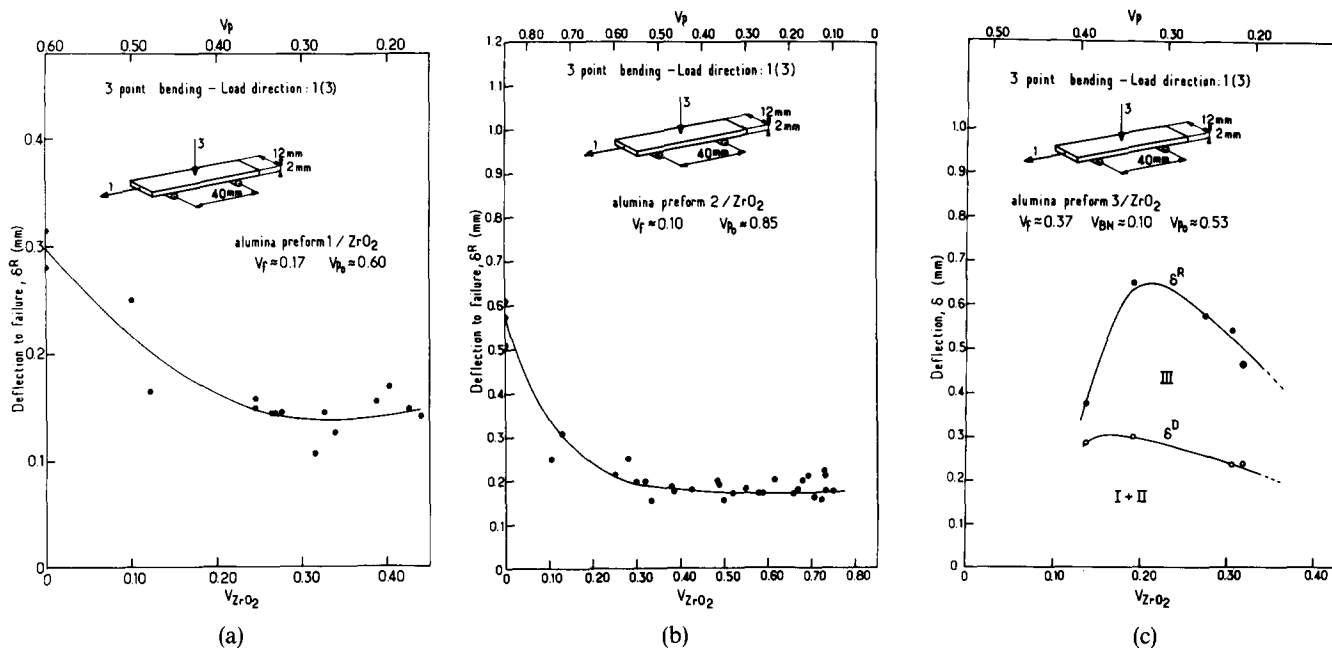

Fig. 8. Variations of the deflection at failure (δ^R) as a function of $V(ZrO_2)$ three-point bending test) for (a) composites type 1, (b) composites type 2, (c) composites type 3.
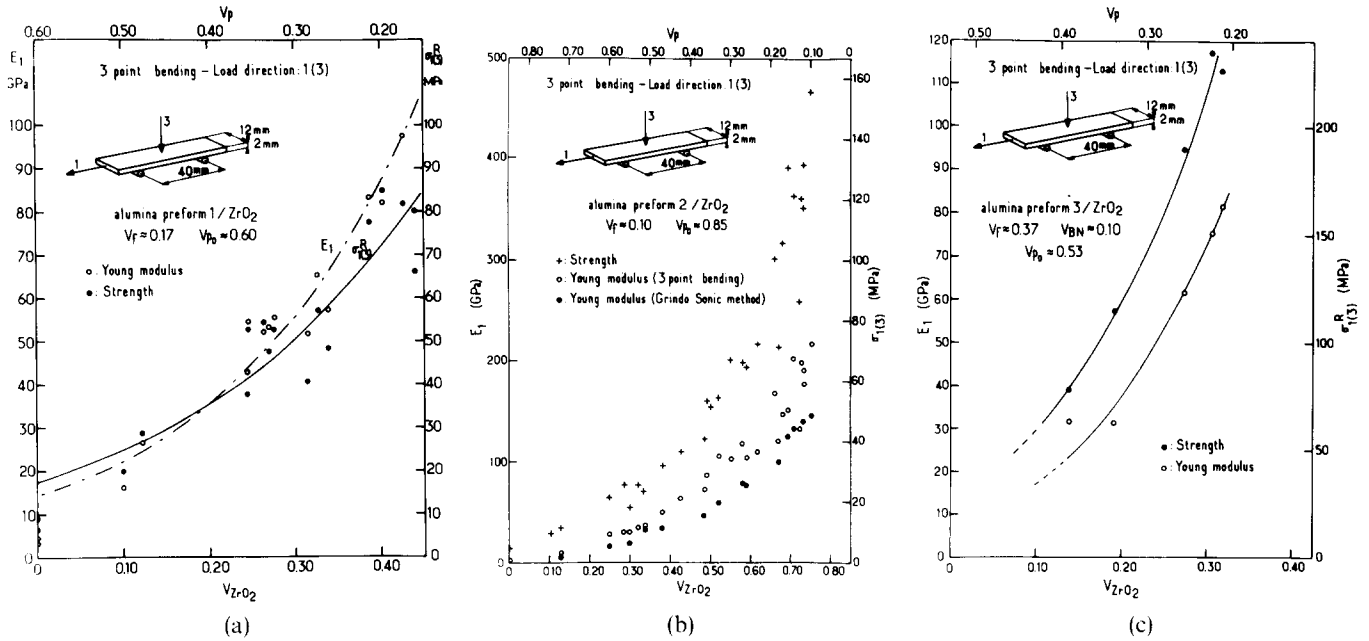
Fig. 9. Variations of bending stiffness and strength versus $V(ZrO_2)$ for (a) composites type 1, (b) composites type 2, (c) composites type 3.

Obviously, the maximum values of the rigidity and bending strength cannot be used alone to work out the influence of the components (fibers, binder, matrix) and fiber architecture on the mechanical behavior of the composites since each composite differs from the others by several parameters. However, it is noteworthy that the rigidities of the three composites are very similar for the same residual porosity (e.g. for $V_p \approx 0.20$, $E_1 \approx 90$–110 GPa), the only slight differences between them being related to the zirconia contents. On the other hand, at equal residual porosities (e.g. $V_p \approx 0.20$), the rupture strength of composites type 3 (with continuous reinforcement) is much higher than those corresponding to composites types 1 and 2 (with a nonwoven reinforcement) whatever the value of $V(ZrO_2)$.

3.2.2.2 Stiffness and strength at high temperatures
The effect of temperature on the rigidity of a composite of type 1 (with $V(ZrO_2) \approx 0.20$) was

Table 3. Coefficients of the exponential evolution of rigidities and rupture strength versus the porosity volume fraction V_p for alumina and carbon reinforced zirconia–matrix composites

Composite	K_{E_1}	$E_1(o)$ (GPa)	K_1^R	$\sigma_1^R(o)$ (MPa)
Type 1	4·46	212	3·56	147
Type 2	5·42	448	4·19	209
Type 3	5·84	273	6·16	893
Type 4	5·07	40·4	6·54	367
Type 5	4·88	47·7	4·28	242

studied within the temperature range 0–1200°C. Young's modulus E_1 values were derived from the measurements of the frequency of acoustic waves propagating at high temperatures along direction 1 of the composites. As shown in Fig. 10, during the first heating, E_1 decreases from 55 to 45 GPa and the material retains this rigidity after cooling to room temperature and after any additional heating. Therefore, the composite seems to have been stabilized during the first treatment at high temperatures by some damaging phenomena that could be related to the thermomechanical fiber–matrix coupling or/and the allotropic transformation of the zirconia matrix (found to occur, in this composite, between 1100 and 1200°C on heating, as shown in Part 2).

The high temperature bending strength was measured from room temperature to 1400°C, on composites types 1 and 3 with zirconia volume
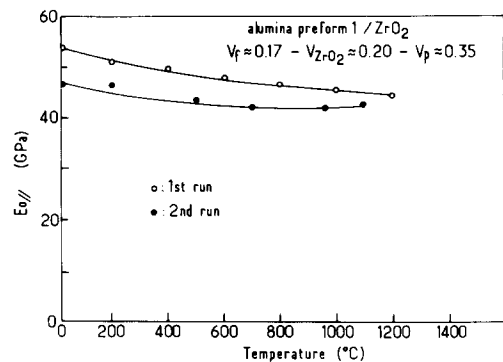

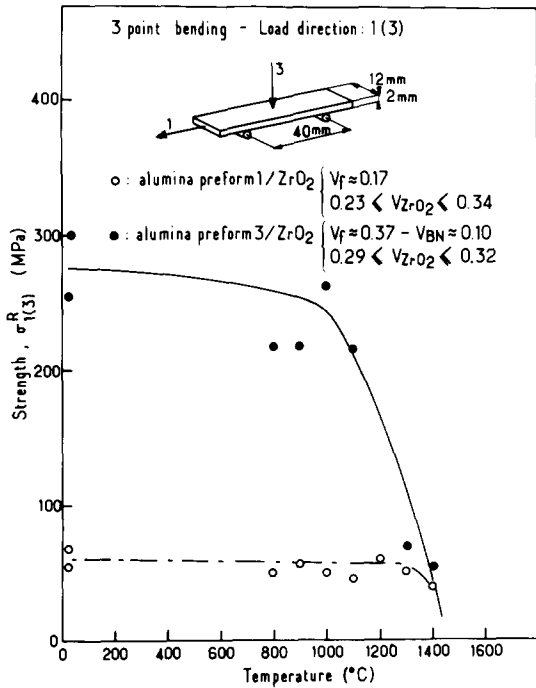**Fig. 10.** High temperature Young's modulus of composites type 1.

Fig. 11. High temperature bending strength of alumina–zirconia composites (types 1 and 3).

fractions within the range 0·25–0·35. The variation of the bending strength as a function of the test temperature is shown in Fig. 11. It appears that the decrease in strength which occurs as the temperature is raised occurs earlier for composites type 3 (i.e. the most resistant at ambient and medium temperatures). Thus, a decrease in strength of 70% is observed between 1300 and 1400°C for the composites type 3 whereas it is only of 30% within the same temperature range for the composites type 1. This difference may be justified by the fact that the Sumitomo alumina-based fibers have a much higher silica content than the Saffil fibers (i.e. 15 and 3 wt % respectively).[16,17] Although the bending strength of the two types of composites are nearly the same at 1400°C (i.e. ≈ 40 MPa), that of the composites type 3 (reinforced by alumina fabric layers) remains at 1000°C about four times higher than the bending strength of the composites type 1 (derived from the mat preform).

3.2.3 Discussion

From the above experimental results, it appears difficult to indicate the influence of each material parameter, on the mechanical behavior of the composites, due to the fact that several parameters are usually simultaneously modified when moving from one given material to another (e.g. fiber and preform natures, fiber–matrix bonding, $V(ZrO_2)$, V_p). This is the result of : (i) a very limited fiber or fibrous semi-product choice (e.g. the Saffil fiber is not

available as a continuous material) and (ii) processing considerations (as mentioned above, in CVI, increasing $V(ZrO_2)$ results in a decrease in V_p and vice versa, for a given initial preform).

Nevertheless, the above results clearly show that among the three composites studied, only one, namely composite type 3, appears to exhibit simultaneously the following positive features: (i) non-brittle behavior due to the presence of a BN-interphase (which is relatively compliant with respect to both the alumina fibers and zirconia matrix, thus enhancing the heterogeneity of the material) which reduces the stress concentration in the vicinity of the fiber surface due to matrix microcracking and enables microcrack deviations and fiber pull-out as shown in Fig. 12, (ii) a sufficient volume fraction of fibers (i.e. $V_f \approx 0.40$) allowing the fibers to support the load relaxation when the matrix undergoes microcracking and (iii) the orientation of a significant part of the reinforcement in the load direction (i.e. nearly half the fiber volume fraction).

On the other hand, the alumina-based binders
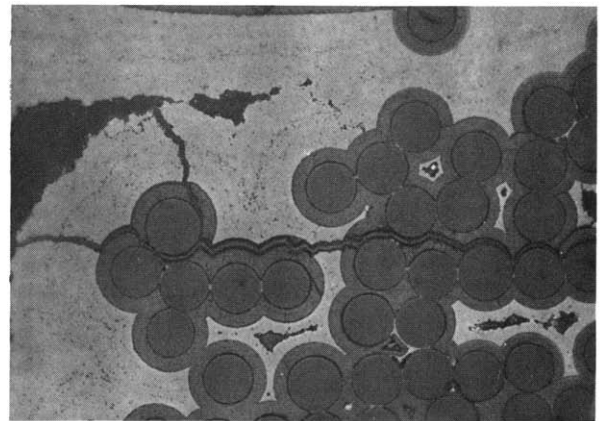
(a)
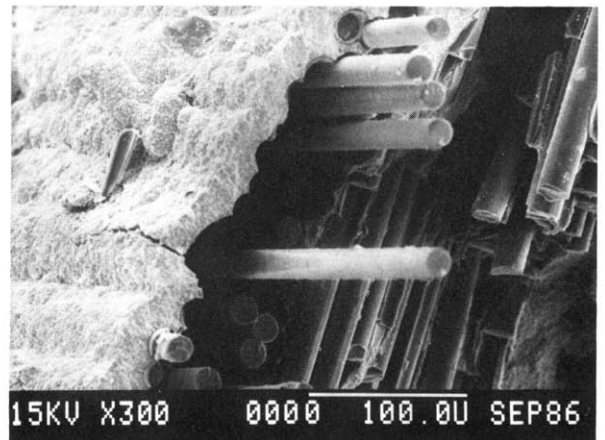
(b)

Fig. 12. Damage and rupture of a composite type 3 ($2D-Al_2O_3$ (Sumitomo)-BN/ZrO_2). (a) Optical micrograph (original magnification × 500), (b) SEM fractograph.
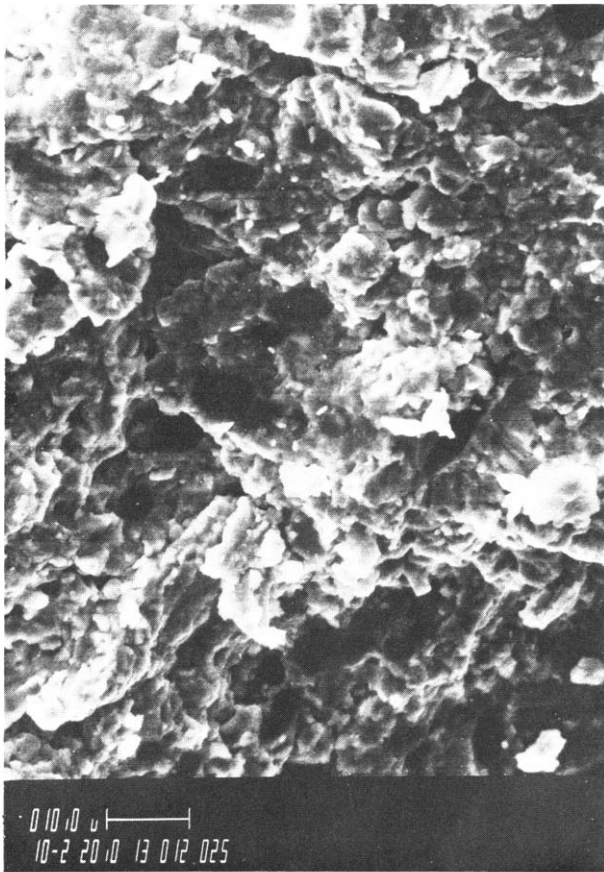
Fig. 13. SEM fractograph of a composite type 1.

which have been used to consolidate the preforms of the composites types 1 and 2 do not obviously play a similar role of compliant interphase. The strong fiber–matrix bonding prevents any fiber pull-out phenomena and results in catastrophic crack propagations as illustrated in Fig. 13.

Although the mechanical behavior of the composites type 3 is good at ambient and medium temperatures, as illustrated in Fig. 11, it will have to be improved at $T > 1000°C$ by, for example, considering more suitable ceramic fibers. This matter remains an open subject since there is presently a well-known lack of thermally stable ceramic fibers (others than carbon fibers).

3.3 Effect of the architecture and carbon coating of carbon fibrous preforms on bending properties

The mechanical behavior of the carbon–zirconia composites (types 4 and 5) was also evaluated under bending with the same testing conditions used for the other zirconia–matrix composites; the load being applied in direction 3. The load-deflection curves obtained for various densification levels are given in Fig. 14.

For both types of composite (4 and 5), the load-deflection curves show similar features although the levels of load are quite different. Up to deflections of
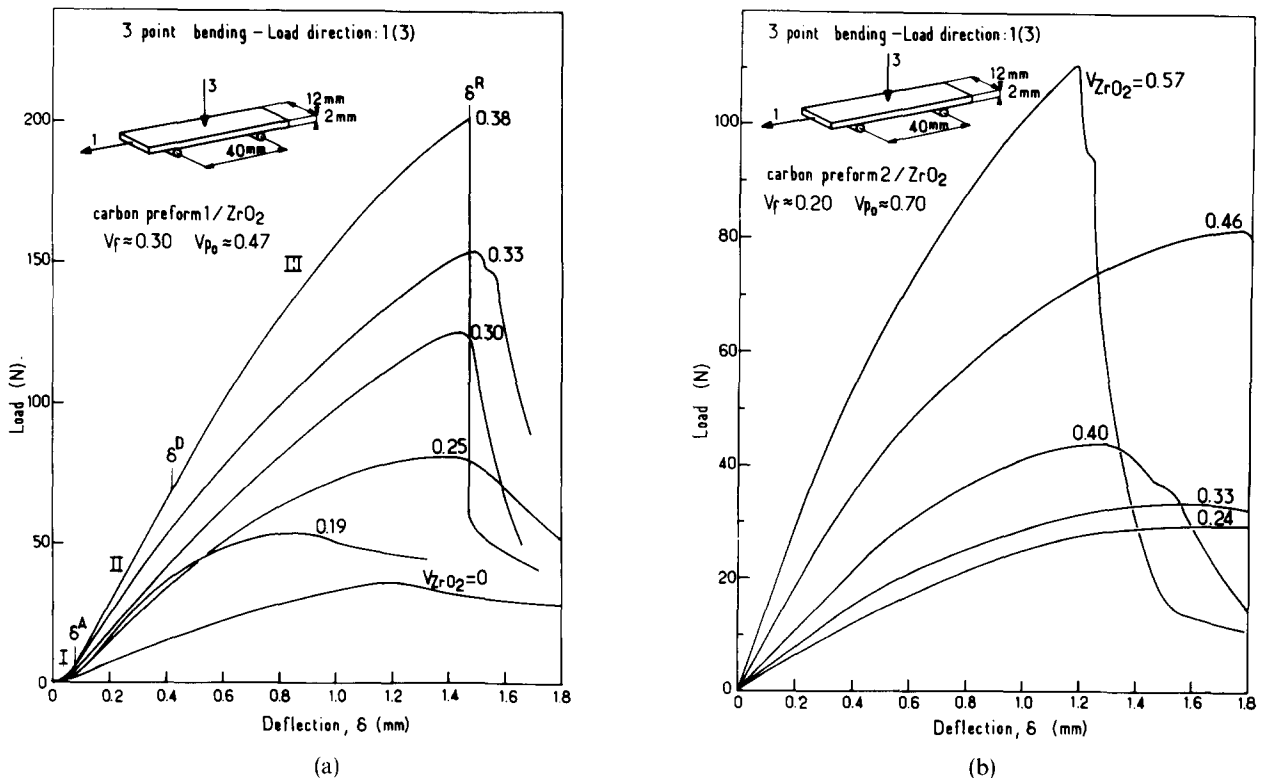

(a)

(b)

Fig. 14. Three-point bending behavior of (a) composites of type 4 (2D-C-C/ZrO₂), (b) composites type 5 (p-3D-C-C/ZrO₂).
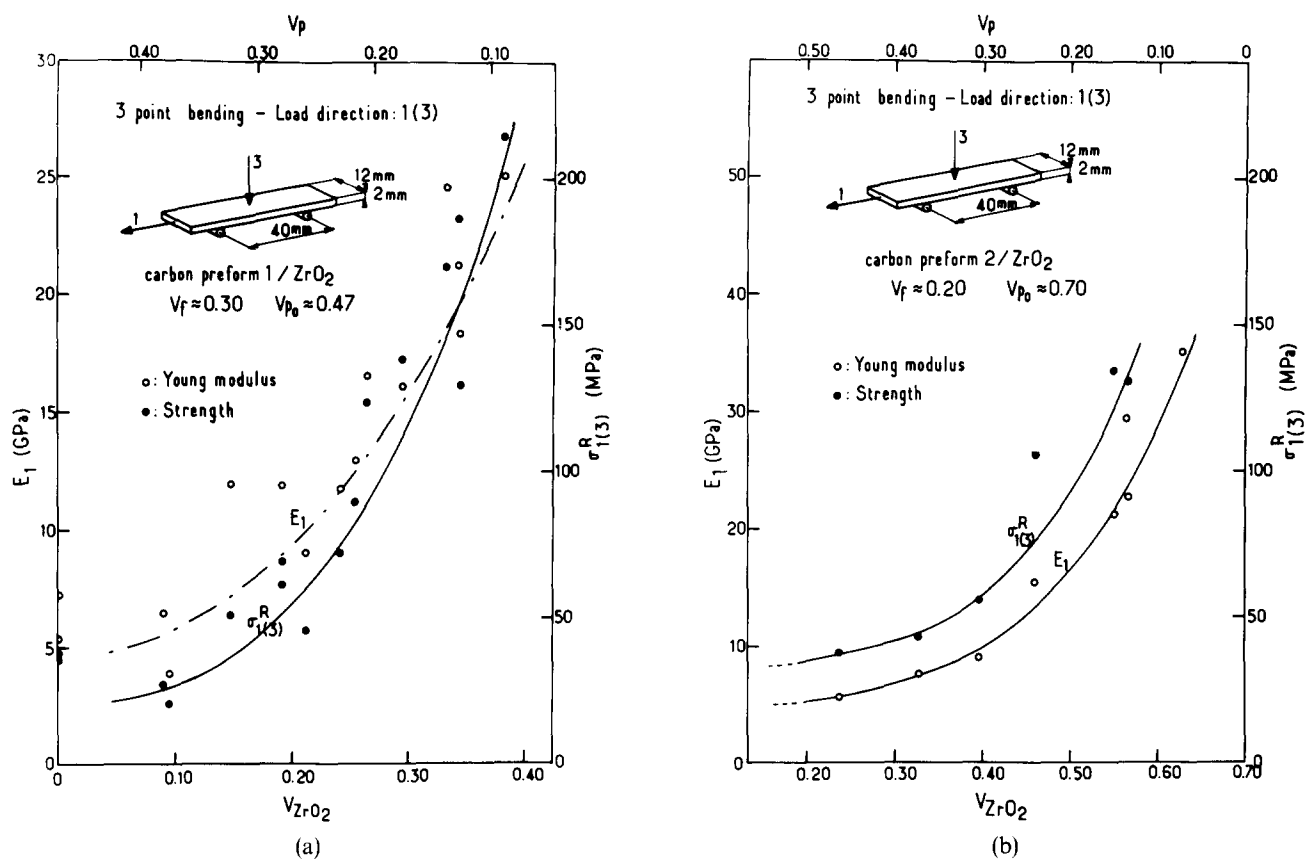
Fig. 15. Variations of the Young's modulus and bending strength versus $V(ZrO_2)$ for (a) composites type 4 (2D-C-C/ZrO_2, (b) composites type 5 (p-3D-C-C/ZrO_2).

about 0·4 mm the composites C-C/ZrO_2 exhibit quasi-linear elastic behavior followed by a widely spread damaging domain preceding the failure.

Furthermore, the increases in stiffness and bending strength versus $V(ZrO_2)$, as illustrated in Fig. 15, are quite similar to those observed for alumina reinforced composites (types 1, 2 and 3). Again, the evolutions can be represented by exponential functions whose coefficients are given in Table 3.

In fact, composites 4 and 5 can be distinguished by their mode of failure which results in some differences in the evolution of the deflection at failure σ^R versus $V(ZrO_2)$ as illustrated in Fig. 16. As long as $V(ZrO_2)$ remains low ($<20\%$) the composites type 4 fail by delamination so that an increase in $V(ZrO_2)$ gives the fabric layer a higher notch sensitivity during buckling of the specimen layers under compression. This results in an embrittlement effect on the densification. As soon as $V(ZrO_2)$ is high enough ($>20\%$) the failure occurs by intralayer crack propagation. The amount of ZrO_2 is sufficient to build up bridging through the fabric layers, impeding any delamination. The rupture is initiated by the fiber fractures in the first fabric layer of the specimen surface under tension. As a matter of fact, the thickness of the carbon

matrix is significant enough to inhibit the notch effects due to zirconia microcracking (Fig. 17). Also, the specimen deflection at failure remains quasi-constant versus $V(ZrO_2)$, since it is related to the tensile fracture strain of the first fiber layer. Thus, the transition in the failure mode of composites type 4 explains the non-monotonous evolution of the rupture deflection versus $V(ZrO_2)$.

On the other hand, the smaller fiber volume fraction and thinner carbon coating in composites type 5 ($V_f = 0·20$; $V_{pyc} = 0·1$) compared to composites type 4 ($V_f = 0·3$; $V_{pyc} = 0·2$) enhance the material sensitivity to the notch effect. The stress concentrations due to microcracking in particularly thick ZrO_2 coatings, control the composite failure. This mode of failure results in a decrease in the rupture deflection as $V(ZrO_2)$ is raised.

Otherwise, the evolution of the bending strength versus temperature shown in Fig. 18 shows for both types of composites (4 and 5) a slight increase in their performance up to about 1000°C.

In summary, the results which have been obtained on the C/ZrO_2 composites are consistent with those already published on other ceramic matrix composites derived from the same carbon preforms (e.g. 2D-C-C/SiC, 2D-C-C/TiC, 2D-C-C/B_4C or 2D-C-
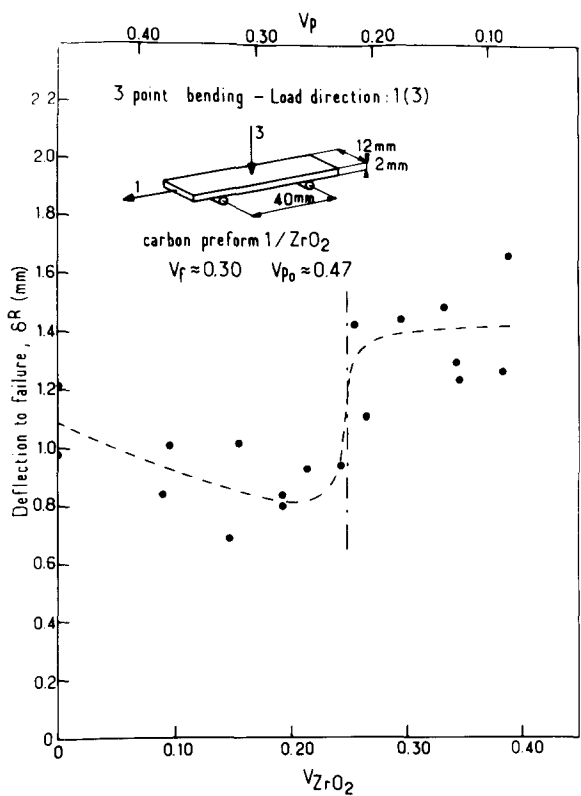
(a)
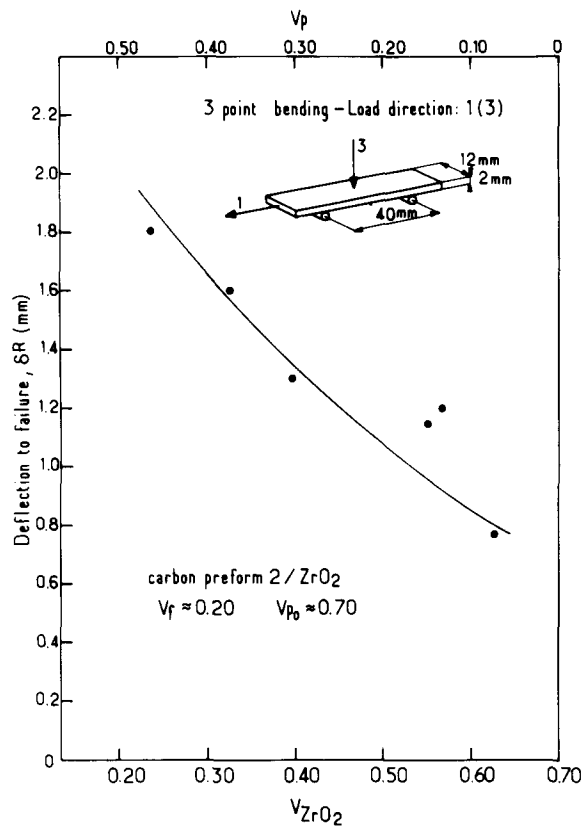
(b)

Fig. 16. Variations of the deflection at failure versus $V(ZrO_2)$ for (a) composites type 4 (2D-C-C/ZrO_2), (b) composites type 5 (p-3D-C C/ZrO_2).

Fig. 17. SEM fractography of a composite type 4.
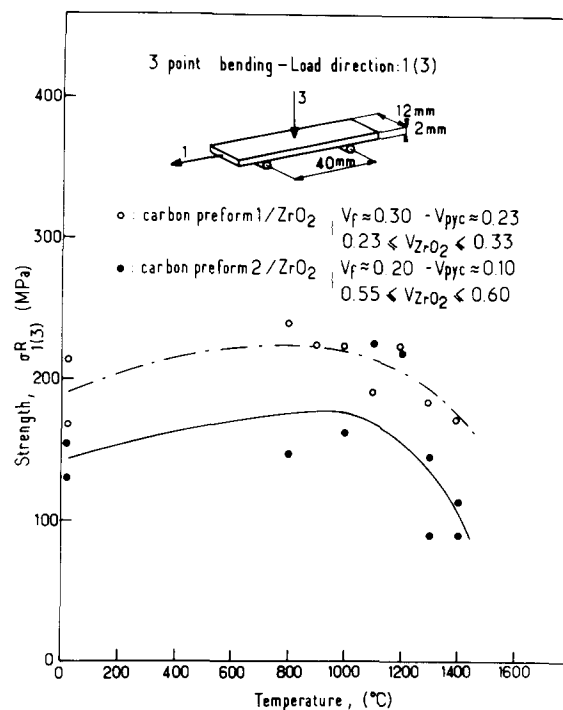

Fig. 18. Evolution of the bending strength versus temperature for composites types 4 and 5.

C/BN) whose comparative properties have been discussed in detail elsewhere.[24,25] Furthermore, and as it will be discussed in Part 2, the interest of carbon fiber reinforced zirconia is limited to specific applications due to the fact that: (i) carbon reacts with oxygen-containing atmospheres above 500°C, (ii) carbon–zirconia reactions may take place in the solid state at high temperatures and (iii) carbon and zirconia are characterized by very different CTE. On the other hand, carbon fibers are currently the best reinforcement for high temperature applications due to their refractoriness and high temperature strength.

Acknowledgements

References

1. Brennan, J. J., Interfacial characterization of glass and glass–ceramic matrix/Nicalon SiC fiber composites. In *Tailoring Multiphase and Composite Ceramics*, ed. R. E. Tressler, G. L. Messing, C. G. Pantano & R. E. Newnham. *Mat. Sci. Res.*, **20** (1986) 549–70.

2. Bender, B., Shadwell, D., Bulik, C., Incorvati, L. & Lewis, D. III, Effect of fiber coatings and composite processing on properties of zirconia-based matrix SiC fiber composites. *Ceram Bull.*, **65**(2) (1986) 363–9.

3. Rice, R. W., BN coating of ceramic fibers for ceramic fiber composites. US patent 4 642 271, 10 February 1987.

4. Singh, R. N. & Brun, M. K., Effect of boron nitride coatings on fiber–matrix interactions. *Ceram. Engng. Sci. Proc.*, **8**(7–8) (1987) 636–43.

5. Prewo, K. M., Brennan, J. J. & Layden, G. K., Fiber reinforced glasses and glass-ceramics for higher performance applications. *Ceram. Bull.*, **65**(2) (1986) 305–13.

6. Minet, J., Langlais, F., Naslain, R. & Bernard, C., On the CVD of zirconia from ZrCl₄–H₂–CO₂–Ar gas-mixture: 1— A thermodynamic approach. *J. Less-Common Met.*, **119** (1986) 219–35.

7. Minet, J., Langlais, F. & Naslain, R., On the CVD of zirconia from ZrCl₄–H₂–CO₂–Ar gas-mixture: 2—An experimental approach. *J. Less-Common Met.*, **132** (1987) 273–87.

8. Minet, J., Langlais, F. & Naslain, R., Chemical vapor infiltration of zirconia within the pore network of fibrous ceramic materials, from ZrCl₄–H₂–CO₂. *Comp. Sci. Techn.*, **37** (1990) 79–107.

9. Colmet, R., L'Hermitte-Sebire, J. & Naslain, R. Fibrous alumina–alumina composite materials obtained according to a CVI-technique. *Adv. Ceram. Mater.*, **1**(2) (1986) 185–91.

10. Fitzer, E. & Gadow, R., Fibre reinforced composites via the sol/gel route. In *Tailoring Multiphase and Composite Ceramics*, ed. R. E. Tressler, G. L. Messing, C. G. Pantano & R. E. Newnham. *Mat. Sci. Res.*, **20** (1986) 571–607.

11. Pujari, V. K. & Jawed, I., The alumina fibre/tetragonal zirconia polycrystal composite system. *Composites*, **17**(2) (1986) 137–40.

12. Claussen, N. & Petzow, G., Whisker reinforced zirconia-

13. Claussen, N. & Petzow, G., Whisker-reinforced oxide ceramics. *J. de Physique*, Colloque C1, Suppl. No. 2, **47** (1986) C1-693–C1-702.

14. Grewe, H., Dreyer, K. & Kolaska, J., Whisker reinforced ceramics. cfi/Ber., 8/9 (1987) 303–17.

15. Marshall, D. B., Lange, F. F. & Morgan, P. D., High strength zirconia fibers. *J. Am. Ceram. Soc.*, **70**(9) (1987) C187–C188.

16. Birchall, J. D., The preparation and properties of polycrystalline aluminum oxide fibers. *Trans. J. Br. Ceram. Soc.*, **82** (1983) 143–5.

17. Abe, Y., Horikiri, S., Fujimura, K. & Ichiki, E., High performance alumina fiber and alumina/aluminium composites. In *Progress in Science and Engineering of Composites*, ed. T. Hayashi *et al.*, Ed. ICCM-IV, Tokyo, 1982, pp. 1427–33.

18. Hannache, H., Naslain, R. & Bernard, C., Boron nitride chemical vapour infiltration of fibrous materials from BCl₃–NH₃–H₂ or BF₃–NH₃–H₂ mixtures: a thermodynamical and experimental approach. *J. Less-Common Met.*, **95** (1983) 221–46.

19. Broquere, B., Buttazzoni, B. & Choury, J. J., Les composites carbone–carbone, leurs applications industrielles. In *Introduction aux Matériaux Composites: 2—Matrices Métalliques et Céramiques*, ed. R. Naslain. CNRS-IMC Editions, Bordeaux, Chap. 17, 1985, pp. 405–38.

20. Christin, F., Naslain, R. & Bernard, C., A thermodynamic and experimental approach of silicon carbide CVD. Application to the CVI-infiltration of porous carbon-composites. *Proc. Int. Conf. CVC*, ed. T. O. Sedwick & H. Lydtin. The Electrochemical Society, Princeton, 1979, pp. 499–514.

21. Naslain, R. & Langlais, F., CVD-processing of ceramic–ceramic composite materials. In *Tailoring Multiphase and Composite Ceramics*, ed. R. E. Tressler, G. L. Messing, C. G. Pantano & R. E. Newnham. *Mat. Sci. Res.*, **20** (1986) 145–64.

22. Rossignol, J. Y., Langlais, F. & Naslain, R., A tentative modelization of titanium carbide CVI within the pore network of two-dimensional carbon–carbon preforms. In *Proc. Int. Conf. CVD (CVC-IX, Cincinnati*, ed. Mc. D. Robinson *et al.* The Electrochemical Society, Pennington, 1984, pp. 596–614.

23. Hannache, H., Langlais, F. & Naslain, R., Kinetics of Boron carbide chemical vapour deposition and infiltration. *Proc. 5th European Conf. on CVD*, ed. J. O. Carlsson *et al.* Uppsala, Sweden, 1985, p. 219.

24. Naslain, R., Quenisset, J. M., Rossignol, J. Y., Hannache, H., Lamicq, P., Choury, J. J., Heraud, L. & Christin, F., An analysis of the properties of some ceramic–ceramic composite materials obtained by CVI-densification of 2D-C-C preforms. In *Proc. 5th Int. Conf. Composite Mater. (ICCM-V, San Diego)*, ed. W. C. Harrigan, J. Strife & A. K. Dhingra. TMS-AIME, Warrendale, 1985, pp. 499.

25. Rossignol, J. Y., Quenisset, J. M., Hannache, H., Mallet, C., Naslain, R. & Christin, F., Mechanical behavior in compression loading of 2D-composite materials made of carbon fabrics and a ceramic matrix. *J. Mat. Sci.*, **22** (1987) 3240–52.

26. Spriggs, R., *J. Am. Ceram. Soc.*, **44** (1961) 628.

27. Rossignol, J. Y., Quenisset, J. M. & Naslain, R., Mechanical behavior of 2D-C-C/TiC composites made of a 2D-C-C preform densified with TiC by CVI. *Composites*, **18**(2) (1987) 135–44.

28. Ryshkewitch, E., Compression strength of porous sintered alumina and zirconia. *J. Am. Ceram. Soc.*, **36**(2) (1953) 65–8.

29. Duckworth, W., Discussion of Ryshkewitch paper by Winston Duckworth. *J. Am. Ceram. Soc.*, **36**(2) (1953) 68.